
ImpMIA: Leveraging Implicit Bias for Membership Inference Attack

Yuval Golbari^{*1} Navve Wasserman^{*1} Gal Vardi¹ Michal Irani¹

Project page: <https://yuvalgol123.github.io/ImpMIA>

Abstract

Determining which data samples were used to train a model, known as Membership Inference Attack (MIA), is a well-studied and important problem with implications on data privacy. SotA methods (which are black-box attacks) rely on training many auxiliary reference models to imitate the behavior of the attacked model. As such, they rely on assumptions which rarely hold in real-world settings: (i) the attacker knows the training hyperparameters; (ii) all available non-training samples come from the same distribution as the training data; and (iii) the fraction of training data in the evaluation set is known. We show that removing these assumptions significantly harms the performance of black-box attacks. We introduce *ImpMIA*, a Membership Inference Attack that exploits the *Implicit Bias* of neural networks. Building on the maximum-margin implicit bias theory, *ImpMIA* uses the Karush–Kuhn–Tucker (KKT) optimality conditions to identify training samples – those whose gradients most strongly reconstruct the trained model’s parameters. Our approach is optimization-based, and requires NO training of reference-models, thus removing the need for any knowledge/assumptions regarding the attacked model’s training procedure. While *ImpMIA* is a white-box attack (a setting which assumes access to model weights), this is becoming increasingly realistic given that many models are publicly available (e.g., via Hugging Face). *ImpMIA* achieves SotA performance compared to both black and white box attacks in settings where only the model weights are known, and a *superset* of the training data is available.

^{*}Equal contribution ¹Department of Computer Science and Applied Mathematics, Weizmann Institute of Science, Rehovot, Israel. Correspondence to: Yuval Golbari <yuval.golbari@weizmann.ac.il>.

Preprint. February 26, 2026.

1. Introduction

Ensuring that trained models do not leak information about their training sets is a critical challenge. Membership inference attacks (MIAs) evaluate this risk by determining whether a given example was part of a model’s training data. MIAs can be broadly divided into two categories: black-box, which assume only query access to model outputs (Shokri et al., 2017; Yeom et al., 2018; Li & Zhang, 2021; Carlini et al., 2022; Wu et al., 2024; Peng et al., 2024), and white-box, which exploit access to internal parameters such as weights or gradients (Nasr et al., 2019; Leino & Fredrikson, 2020; Cohen & Giryas, 2024; Suri et al., 2024).

The most effective black-box MIAs are reference-model-based attacks. These methods estimate the distribution of losses for members (training samples) versus non-members by training auxiliary reference models that mimic the target model, thereby learning its loss behavior. However, training large sets of reference models is computationally expensive, and—more importantly—their effectiveness depends on the reference models being accurate surrogates of the target. As a result, these attacks rely on several strong assumptions: (i) the attacker knows the training hyperparameters (e.g., learning rate, optimizer, number of epochs); (ii) the non-training samples come from the same distribution as the training data; and (iii) the fraction of training members in the evaluation set is known. When any of these assumptions is violated, the performance of black-box MIAs drops significantly (Shokri et al., 2017; Salem et al., 2019; Song & Mittal, 2021; Carlini et al., 2022), limiting their reliability for auditing privacy.

On the other hand, white-box MIAs assume access to model weights or gradients. While this is a restrictive assumption, this scenario is increasingly realistic, as many modern models are released with their parameters publicly available (e.g., via platforms such as Hugging Face). White-box MIAs have shown strong performance by leveraging gradients and activations (Nasr et al., 2019; Leino & Fredrikson, 2020), or influence scores (Cohen & Giryas, 2024). However, despite these advances, current white-box attacks still lag behind the best black-box approaches when evaluated under stringent criteria such as the true-positive rate (TPR) at very low false-positive rates (FPR), which has been suggested as a reliable evaluation criterion by Carlini et al. (2022).

We propose *ImpMIA*, a white-box membership inference attack that is the first to adapt neural network *Implicit-Bias* theory for this task (see Approach Overview in Fig. 1). Unlike prior approaches, our attack does not rely on training any reference models, and is therefore unaffected by the common assumptions in reference-model methods. *ImpMIA* requires no knowledge of the target model’s training procedure or data distribution, operating in a no auxiliary-knowledge scenario where only the model weights are known, and a *superset* of the training data is available.

Our attack builds on the implicit-bias theory in neural nets, which shows that gradient-based optimization tends to converge to solutions that satisfy the Karush–Kuhn–Tucker (KKT) optimality conditions of a certain maximum-margin problem (Lyu & Li, 2019; Ji & Telgarsky, 2020). In practice, this implies that the trained parameters of a network can be approximately expressed as a linear combination of per-sample gradients from the training set. Given a set of candidate samples and the trained network weights, we *optimize* a set of coefficients—one per sample—that best reconstructs the network parameters. This provides the key signal: training samples are expected to receive significantly larger coefficients, while non-members remain small.

ImpMIA is best suited for scenarios where the training-set is contained in the examined-set. Such scenarios are relevant, e.g., if one wants to check whether their own dataset has been used for training a model, or when a dataset is *known* to contain the training-set (e.g., a publicly available dataset), but not which part of it was used for training. While this is a somewhat restrictive assumption, we show that it can be relaxed (App. B.3), and that our performance is competitive even at low coverage of the training-set (only 10%), and becomes superior at high coverage.

ImpMIA achieves superior results, surpassing both black-box and white-box attacks under no auxiliary-knowledge settings across 3 benchmark datasets. Our extensive analysis shows that removing the knowledge assumptions made by most reference-model-based methods (knowledge of the attacked model’s training procedure & setting), leads to a significant drop in performance of SotA methods, while our attack remains unaffected. Altogether, these results highlight the importance and effectiveness of our proposed method as a practical membership inference attack.

Our contributions are as follows:

- We introduce *ImpMIA*, the first membership inference attack based on the implicit bias of gradient descent and its corresponding KKT conditions.
- *ImpMIA* achieves SotA performance in scenarios where only model weights & a candidate data pool are available.
- We provide a systematic evaluation of the robustness of leading MIA methods in settings where training hyperparameters, data distribution, or member ratios are unknown.

2. Related Work

2.1. Membership inference

Membership Inference Attacks (MIAs) are divided into black-box attacks, which rely on model outputs, and white-box attacks, which exploit access to model parameters.

White-box attacks exploit access to a model’s internal parameters (often gradients) to amplify membership signals. Nasr et al. (2019) introduced one of the first frameworks, leveraging activations and per-example gradients. Sablayrolles et al. (2019) derived the Bayes-optimal test under white-box access, showing that maximum membership power can be achieved by computing likelihood ratios over model parameters. Leino & Fredrikson (2020) showed in their Stolen Memories attack that gradient norms alone provide strong membership signals, and that training an auxiliary classifier to distinguish gradients from members versus non-members further improves accuracy. Most recently, Cohen & Giryes (2024) proposed a self-influence attack that uses influence functions to measure each sample’s effect on its own loss, combined with the predicted label. While white-box access is a strong assumption, it is increasingly realistic as many modern models are released with their full weights (e.g., on Hugging Face).

Black-box MIAs assume the attacker can only query the target model and observe its outputs. Shokri et al. (2017) introduced the shadow-model framework, training reference models to mimic the target and then learning an attack model from their outputs. Yeom et al. (2018) later showed that even without reference models, the simple “gap” heuristic, predicting membership when the model’s output label matches the ground truth, can be effective. Li & Zhang (2021) proposed decision-based attacks relying on adversarial perturbations, while Ye et al. (2022) introduced *Attack-P*, a population-based loss thresholding method, and *Attack-R*, a sample-specific calibration using percentiles from reference models for improved robustness. Building on the reference-model paradigm, Carlini et al. (2022) proposed LiRA, which compares target losses to reference-model distributions and emphasized low false-positive evaluation. Zarifzadeh et al. (2023) (RMIA) further refined LiRA with an optimized likelihood-ratio test, improving efficiency under strict computational limits. LiRA and RMIA currently represent the strongest-performing black-box MIAs.

Limitations of Reference-Model Attacks. Reference-model attacks are costly to train and their effectiveness depends heavily on how these models are trained. Specifically, three key assumptions; whose violation significantly reduces MIA performance: (i) **Knowledge of the target model’s training hyperparameters** (e.g., learning rate, optimizer, epochs): Jayaraman et al. (2021) and Carlini et al. (2022) (LiRA) reported accuracy drops when altering those hyperparameters, while Pradhan et al. (2025) propose meth-

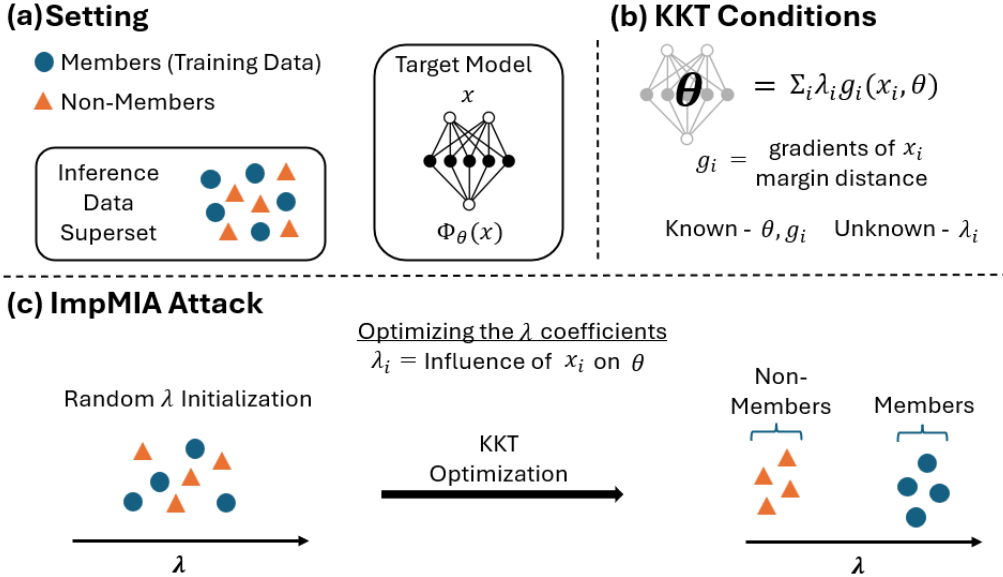


Figure 1. **Overview of the Approach.** (a) Setting: Given a trained model with parameters θ and a candidate superset containing training members (blue) and non-members (orange), the adversary’s goal is to identify which samples are members. (b) KKT conditions: Our attack builds on implicit bias theory, which shows that gradient-based optimization converges to solutions satisfying the Karush–Kuhn–Tucker (KKT) conditions of the maximum-margin problem. Since weights are known and gradients are computable, only the coefficients remain unknown. (c) ImpMIA: We optimize one coefficient per sample to best reconstruct the model parameters, where members are expected to receive large coefficients and non-members small ones.

ods to partially mitigate this hyperparameters sensitivity, but rely on additional reference models and distributional assumptions. (ii) **Matching data distribution:** Salem et al. (2019) and Shi et al. (2024) show degraded accuracy when shadows were trained on different domains (e.g., CIFAR-10 for a CIFAR-100 target). (iii) **Member ratio in the inference pool:** Jayaraman et al. (2021) and Song & Mittal (2021) found inflated false positives and reduced accuracy when this assumption was wrong. In this work, we systematically test these factors showing significant drops across models on CIFAR-10, CIFAR-100, and CINIC-10. Such scenarios where these factors are *unknown* to the attacker are common as models, particularly those trained on sensitive data, are unlikely to publish this information.

2.2. Implicit Bias of Gradient Descent

In overparameterized neural networks, one might expect overfitting the training data. Yet gradient-based methods tend to converge to classifiers that generalize well to new unseen data (Zhang et al., 2021; Neyshabur et al., 2017). This phenomenon is explained by the *implicit bias* of training algorithms: gradient descent tends to prefer specific solutions, and characterizing these has been central to deep-learning theory in recent years (see Vardi (2023) for a survey). For homogeneous ReLU networks trained to zero logistic or cross-entropy loss, Lyu & Li (2019) and Ji & Telgarsky (2020) showed that the learned weights necessarily satisfy the *KKT conditions* of a maximum-margin problem. Building on this, Haim et al. (2022) demonstrated that networks trained with binary cross-entropy allow reconstruction of

dozens of nearly pixel-perfect training samples. This was later extended to multiclass classifiers (Buzaglo et al., 2023) and more realistic transfer-learning workflows (Oz et al., 2024). All of these data reconstruction attacks are limited to very small datasets (up to a few thousand examples), and require simple models (mostly MLPs). In this work, we adapt the implicit-bias approach for the first time to membership inference attack, identifying which samples from a candidate pool best satisfy the KKT conditions.

3. Preliminaries

3.1. Membership Inference Attack Setting

Membership inference attacks (MIAs) aim to determine which data points were part of the training set of a machine learning model. The strongest recent black-box methods are reference-model based, and they rely on additional assumptions about the target model’s training configuration and the candidate set, which are unlikely to hold in practice. In this work, we focus on a scenario where the adversary has access only to a superset that contains the training set (or part of the training set) and to the model weights. This reflects real-world conditions: modern models are often released publicly with their weights, while auditors may possess large candidate pools that include the training set but lack detailed knowledge of the training data distribution or the exact training configuration. Our setting adapts the basic membership inference game (Yeom et al., 2018; Jayaraman et al., 2021), where a single sample is evaluated at a time, into a *set-based* formulation in which the full candidate pool

is attacked and evaluated (similar to the online setting in Carlini et al. (2022); Zarifzadeh et al. (2023)). We assume that the evaluated set contains the training set or at least a portion of it (e.g. more than 10%). While this assumption was not taken in prior work, the reported results in those settings were in fact obtained under it. That is, for technical reasons, their evaluations were obtained in a setting where the attacker uses a superset of the training data (Carlini et al., 2022). Results for our method in a scenario where this assumption is relaxed are presented in App. B.3.

Formally, we study a *set-based* No-Auxiliary-Knowledge setting. Let X_{train} be the (unknown) training set drawn from a distribution \mathcal{D} , and f_θ a model trained on X_{train} . Let X_{sup} be a candidate pool with $X_{\text{train}} \subseteq X_{\text{sup}}$, and the remaining samples being non-members, potentially drawn from other distributions. The adversary is given the trained parameters θ and the pool X_{sup} , but: (i) does not know the target model’s training hyperparameters; (ii) cannot assume non-members are drawn from the same distribution as the training set; and (iii) does not know how many members are in X_{sup} or their ratio. The adversary must then assign a real-valued score to each sample, with membership decisions.

3.2. The Implicit Bias Formulation

In this section, we provide an overview of the KKT conditions and the maximum-margin formulation, following the definitions in Haim et al. (2022); Buzaglo et al. (2023). While the theory described below is formally constrained to homogeneous¹ ReLU networks (Lyu & Li, 2019; Ji & Telgarsky, 2020), we show in practice that the results hold more generally for other architectures. The theoretical results of Lyu & Li (2019); Ji & Telgarsky (2020) consider training without weight decay, but in App. D we show that incorporating weight decay leads to the same final equations, and in App. B.6 we analyze its influence on the attack performance.

Implicit bias of gradient flow on homogeneous networks:

Let $\Phi(\theta; \cdot) : \mathbb{R}^d \rightarrow \mathbb{R}^C$ be a homogeneous ReLU network with logits $\Phi(\theta; x)$. Consider minimizing the cross-entropy loss over a multiclass dataset $\{(x_i, y_i)\}_{i=1}^n \subseteq \mathbb{R}^d \times [C]$ using gradient flow (i.e., gradient descent with a small step size). Suppose that at some time t_0 the network classifies all training samples correctly. Then gradient flow converges in direction to a KKT point of the multiclass maximum-margin problem:

$$\begin{aligned} \min_{\theta} \quad & \frac{1}{2} \|\theta\|^2 \\ \text{s.t.} \quad & \Phi_{y_i}(\theta; x_i) - \Phi_j(\theta; x_i) \geq 1, \\ & \forall i \in [n], \forall j \in [C] \setminus \{y_i\}. \end{aligned} \quad (1)$$

The KKT conditions for the multiclass maximum-margin problem are defined in terms of the pairwise margins. For

¹A model Φ is homogeneous w.r.t. θ if there exists $L > 0$ such that $\forall c > 0, x : \Phi(x; c\theta) = c^L \Phi(x; \theta)$.

each sample i and competing class $j \neq y_i$, define

$$m_{i,j}(\theta) := \Phi_{y_i}(\theta; x_i) - \Phi_j(\theta; x_i). \quad (2)$$

The KKT conditions are then given by:

$$\theta = \sum_{i \in [n]} \sum_{j \in [C] \setminus \{y_i\}} \lambda_{i,j} \nabla_{\theta} m_{i,j}(\theta). \quad (3)$$

$$\begin{aligned} \text{For all } i \text{ and } j \neq y_i : \quad & m_{i,j}(\theta) \geq 1, \\ & \lambda_{i,j} \geq 0, \\ & \lambda_{i,j} = 0 \text{ if } m_{i,j}(\theta) \neq 1. \end{aligned} \quad (4)$$

Equation 3, called the *stationarity condition*, represents the weights as a linear combination of margin gradients (distance between a sample’s true class Φ_{y_i} and other classes Φ_j), while Equation 4 specifies additional constraints. The coefficients are the $\lambda_{i,j}$, defined per sample i per class j . In practice, the distance of a sample x_i to the decision boundary is typically determined by a single competing class j . Following Buzaglo et al. (2023), we therefore simplify the stationarity condition by retaining only the smallest margin:

$$\begin{aligned} m_i^{\min}(\theta) &:= \Phi_{y_i}(x_i; \theta) - \max_{j \neq y_i} \Phi_j(x_i; \theta), \\ \theta &= \sum_{i=1}^m \lambda_i g_i, \quad g_i := \nabla_{\theta} m_i^{\min}(\theta). \end{aligned} \quad (5)$$

While our attack builds on the same condition as Buzaglo et al. (2023), our goal differs: instead of reconstructing training data $\{x_i\}$, we fix the candidate inputs and optimize only the coefficients $\{\lambda_i\}$ to obtain membership scores.

4. ImpMIA Attack

In this section, we introduce *ImpMIA*, our white-box membership inference attack that exploits the implicit bias of neural networks. The attack builds on the observation from Eq. 5 that trained parameters can be represented as a linear combination of per-sample gradients from the training samples (members). Thus, members can be distinguished from non-members by their relative contribution to this representation of the parameters, where members contribute to this reconstruction while non-members do not. We first outline the practical construction of the attack in Sec. 4.1, and then detail the technical optimization procedures and stabilization strategies in Sec. 4.2.

4.1. Practical Attack Construction

Building on the theoretical link between the KKT stationarity condition and the representation of trained parameters (Eq. 3), we now describe how this insight is used to devise the ImpMIA attack. The KKT stationarity condition guarantees that the trained parameter vector can be expressed as:

$$\theta = \sum_{i \in X_{\text{train}}} \lambda_i g_i,$$

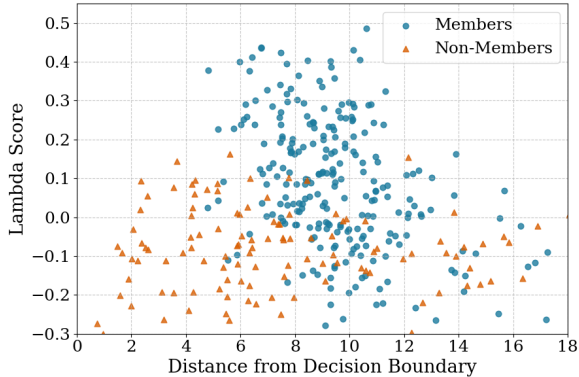


Figure 2. **Lambda scores visualization.** Scatter plot of evaluated samples, with the x-axis showing distance to the decision boundary and the y-axis showing λ scores; points are colored by membership (member vs. non-member). High λ indicates membership.

where each g_i is the margin gradient of a training sample and $\lambda_i \geq 0$ is its corresponding multiplier. The model weights are known hence the per-sample gradients can be computed. Therefore, the only unknowns are the λ coefficients, which can be obtained by optimizing them to satisfy the equation.

In practice, the attacker does not know the true training set, but only has access to a candidate pool $X_{\text{sup}} = \{(x_i, y_i)\}_{i=1}^M$, which contains an unknown subset of training samples X_{train} and non-members X_{test} . However, we can still optimize the coefficients using all samples, deriving a λ coefficient for each (either member or not). This provides the key signal: we expect the coefficients of training samples to be significantly larger, while those of non-members remain small. This is because the number of network parameters is typically much larger than the size of the candidate pool, and therefore deriving the correct weights in the optimization is much more likely when true members exert stronger influence. Importantly, when $|X_{\text{sup}}|$ is smaller than the dimension of θ and the vectors $\{g_i\}$ are linearly independent, the system admits a unique solution for $\{\lambda_i\}$. Note that, following Eqs. (4)-(5), we expect large coefficients for training samples near the margin (close to the decision boundary), while other samples are expected to have lower coefficients (zero in theory).

Formally, for each candidate (x_i, y_i) we compute the multi-class margin gradient

$$g_i = \nabla_{\theta} \left[\Phi_{y_i}(\theta; x_i) - \max_{j \neq y_i} \Phi_j(\theta; x_i) \right],$$

and stack these into the matrix $A = [g_1 \mid \cdots \mid g_M] \in \mathbb{R}^{p \times M}$, where p is the number of model parameters. If the training set were known, we could restrict to A_{train} and solve exactly for multipliers λ_{train} such that $A_{\text{train}} \lambda_{\text{train}} = \theta$. Since the training set is unknown, we instead solve the full system $A \lambda_{\text{score}} = \theta$, deriving M (number of candidates) coefficients. The resulting coefficients are used to calculate a membership score, where large values for a specific sample are interpreted as evidence of a higher prob-

ability that this sample was part of the training data (i.e., a member). To improve robustness and suppress spurious large values from non-members, we incorporate additional techniques for regularization and aggregation (detailed in Section 4.2). In Fig. 2, we present a scatter plot of members and non-members, where the y-axis shows the λ score and the x-axis the sample’s distance from the margin (i.e., $\Phi_{y_i}(x_i; \theta) - \max_{j \neq y_i} \Phi_j(x_i; \theta)$). As illustrated, high λ scores are strong indicators of membership.

4.2. Implementation Details

Given an evaluation set of labeled samples, we optimize the λ coefficients to satisfy the KKT conditions. We first filter out misclassified samples, since training members are more likely to be correctly predicted. For each remaining sample, we include both the original and its horizontal flip, reflecting the fact that most models are trained with augmentations, while keeping computational cost low by not adding further augmentations.

The only optimized variables are the λ coefficients. Therefore, we precompute the margin gradients with respect to the model parameters, forming the columns of the matrix A (as introduced in the previous section). Since A is extremely large (with the number of rows corresponding to the number of network parameters), we split it into blocks for more efficient optimization. Specifically, each block corresponds to roughly 1.5×10^5 parameters, and we optimize the coefficients separately per block. This block partitioning not only reduces memory usage, but also mitigates the ill-conditioning of A : consecutive layers or filters typically share similar statistics, so solving many smaller systems lowers the condition number compared to optimizing the full matrix at once. Moreover, although non-members can obtain a high coefficient due to imperfect optimization, deriving coefficient solutions per block allows averaging across blocks. This improves results, since a sample is unlikely to consistently receive high coefficients in different blocks if it was not part of the training set.

Both the gradient block and the target parameter vector are centered and normalized. For each sample, we then aggregate the optimized coefficients across blocks and augmentations to obtain a final score (see App. A for more details). Our attack is designed to be both memory-efficient and numerically stable, while suppressing noisy scores for non-members.

5. Experimental Setting

We evaluate ImpMIA against both black-box and white-box baselines across CIFAR-10, CIFAR-100, and CINIC-10, using a standard ResNet-18 as the target model. Our experiments reflect realistic adversarial conditions, where the attacker is given only the trained model weights and a superset of the training data, with no knowledge of the training hyperparameters, data distribution, or member ratio.

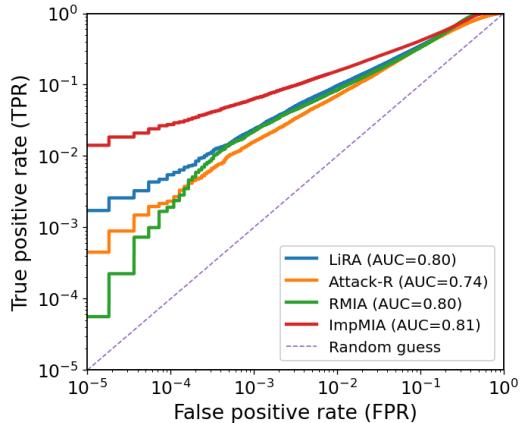


Figure 3. **TPR-FPR in the No-Auxiliary-Knowledge setting (CIFAR-10).** We evaluate a setting with (i) unknown training configuration, (ii) distribution shift in the candidate pool, and (iii) unknown member ratio.

We first describe the datasets, evaluation metrics, and the competing baseline models (Sec. 5.1). We then detail the different scenarios corresponding to the assumptions usually made by reference-model-based MIAs, beginning with the setting where all assumptions are provided, and then moving to a more realistic setting without them (Sec. 5.2).

5.1. Models, Datasets and Evaluation Metrics

For all experiments, the target model is a ResNet-18 trained following the standard recipe of Cohen & Giryès (2024). Specifically, we use a batch size of 100, a learning rate of 0.1, momentum 0.9 with Nesterov acceleration, weight decay of 10^{-4} , and train for 400 epochs using stochastic gradient descent (SGD) with standard data augmentations (random crop and horizontal flip). For each dataset and scenario, we randomly sampled 5 different sets of training samples, and trained 5 target models. Results are averaged across them.

We report performance using both aggregate metrics (AUC) and stringent low-false-positive criterion, True Positive Rate (TPR) at False Positive Rate (FPR) of 0.01% and 0.0%. This criterion was introduced in Carlini et al. (2022), which observed that average-case metrics such as accuracy or AUC can be misleading: an attack may appear strong overall, yet fail completely in the regime of low false positives, which is the regime most relevant for privacy auditing (see App. E for a detailed discussion). In practice, an adversary cannot afford a large number of false alarms, as even a tiny FPR may translate to thousands of incorrectly flagged samples in real-world deployments. Therefore, evaluating TPR at very low FPR provides a stricter and more meaningful measure of membership inference risk.

We compare ImpMIA against recent state-of-the-art black-box and white-box membership inference attacks. For black-box attacks, we include Attack-P (Li & Zhang, 2021), Attack-R (Ye et al., 2022), and focused on the online version of LiRA (Carlini et al., 2022) and RMIA (Zarifzadeh

et al., 2023), which currently represent the strongest black-box MIAs. For black-box baselines, we followed their best setting (e.g. training 256 reference models per experiment). For white-box attacks, we evaluate the adaptive self-influence attack (AdaSIF) (Cohen & Giryès, 2024), which represents the current state of the art in this category (see App. C.2 for additional implementation details). We also include as a baseline a simple white-box attack based on the magnitude of the network gradients, since Nasr et al. (2019) noted that this quantity provides the main signal in their attack (see App. C.2 for additional details). We were unable to compare with Nasr et al. (2019) and Leino & Fredrikson (2020), as their code is not available.

5.2. Membership Inference Attack Scenarios

The basic scenario is the one commonly assumed in black-box attacks, which remain the strongest methods even relative to existing white-box approaches. In the *Full Auxiliary-Knowledge setting*, the attacker is assumed to know both the model architecture and the training hyperparameters used to train the target model (e.g., learning rate, optimizer, epochs). The attacker is also given a pool of samples containing both members and non-members, under the assumptions that (i) the pool is drawn from the same distribution as the training data and (ii) the member/non-member ratio is known, often fixed at 1:1.

These assumptions give reference-model attacks (e.g., LiRA, RMIA) a strong advantage: by training many reference models under identical conditions, they can reconstruct the target model’s member/non-member loss distributions. This explains their strong performance in this regime, though it comes at the cost of training large model ensembles and relies on knowledge rarely available in practice.

To evaluate attack performance under more realistic conditions, we design experimental scenarios that relax these assumptions. In Sec. 6, we present results in the more realistic setting where those assumptions are not made, as well as in each individual scenario where one assumption is removed. Importantly, to ensure fair comparison across scenarios and with prior work, we kept the target model fixed and followed the basic scenario used in previous studies.

The assumption-elimination scenarios are:

- **Unknown Training Configuration** – Since the attacker is not exposed to the target model’s training parameters, we trained the reference models of methods that require them using different settings. Specifically, we used a different batch size (200 instead of 100), learning rate (0.01 instead of 0.1), weight decay (10^{-3} instead of 10^{-4}), and epochs (100 instead of 400) than those used for the ResNet-18 target model (detailed in Sec. 5.1).
- **Different Data Distribution** – In this case, the attacker’s candidate pool mixes in-distribution data (the distribution from which the target model was trained) and out-of-

Attack	CIFAR-10			CIFAR-100			CINIC-10		
	AUC	@0.01 %	@0.0 %	AUC	@0.01 %	@0.0 %	AUC	@0.01 %	@0.0 %
<i>Attack-P</i>	0.76	0.02	0.0	0.89	0.01	0.0	0.83	0.01	0.0
<i>Attack-R</i>	0.74	0.23	0.04	0.95	0.52	0.04	0.83	0.31	0.0
<i>LiRA</i>	0.80	0.55	0.17	0.96	7.90	2.36	0.88	2.27	0.66
<i>RMIA</i>	0.80	0.19	0.01	0.97	6.73	1.22	0.87	0.15	0.03
<i>GradNorm – loss</i>	0.81	0.11	0.01	0.93	0.10	0.04	0.85	0.09	0.01
<i>GradNorm – margin</i>	0.72	0.02	0.0	0.81	0.02	0.01	0.77	0.03	0.01
<i>AdaSIF</i>	0.80	0.05	0.0	0.92	0.01	0.0	0.85	0.01	0.0
Ours	0.81	2.76	1.41	0.95	14.86	5.26	0.87	5.32	2.47

Table 1. **Membership Inference results.** Performance of ImpMIA compared to black-box (LiRA, RMIA) and white-box baselines across 3 datasets under the No-Auxiliary-Knowledge setting. The main relevant metrics are TPR values at fixed false-positive rates (FPR = 0.0% and 0.01%), which capture detection power under stringent error constraints. ImpMIA significantly surpasses all other methods by a wide margin, due to their reliance on the different assumptions. For completeness, we also report AUC as an aggregate measure.

distribution (OOD) data. For each dataset, we construct a pool of $50k$ samples by combining $30k$ in-distribution images with $20k$ OOD images (taken from another dataset). The target model is trained on $25k$ in-distribution samples drawn from the $30k$ portion, allowing for 5 repetitions of the experiment (with 5 different target models). In the reference-based attacks under the relevant online setting, the attacker trains each reference model on half of the evaluation set, i.e., $25k$ examples sampled from the full mixed pool. OOD sources include a subset of ImageNet adapted to CIFAR-10 (CINIC-10 (Darlow et al., 2018)) and an enriched OpenImages dataset (Kuznetsova et al., 2020).

- **Unknown Fraction of Members** – In this case, the attacker does not know the proportion of training members in the candidate pool. The pool is constructed to contain $80k$ examples. Reference-model attacks that assume a 1:1 ratio train their reference models on $40k$ samples (half treated as members and half used to estimate the loss distribution of non-members), while the target model is trained on only $25k$. This mismatch causes the member/non-member loss distributions to differ significantly. We evaluate this scenario individually on CINIC-10, since the other datasets are too small for a meaningful setup.
- **No-Auxiliary-Knowledge Setting** – Combining the above cases, the candidate pool for each dataset has $80k$ samples formed by mixing $30k$ in-distribution with $50k$ OOD images. The attacker trains reference models on a $40k$ -example subset sampled from the full mixed pool under different configurations and without access to the true member ratio.

6. Results

In this section, we quantitatively compare our *ImpMIA* attack against prominent prior black-box and white-box attacks across multiple datasets. In Sec. 6.1, we demonstrate the superiority of our attack in the realistic scenario where

only the model weights are known and the attacker is given a superset of samples that includes the training data, but without any additional knowledge of the model training or the superset composition. Next, in Sec. 6.2, we systematically analyze the impact of eliminating each assumption across different models, showing that reference-model-based methods suffer significant performance drops, while our method remains unaffected.

6.1. Membership Inference Results

We report membership inference attack results across three datasets, demonstrating the superiority of our proposed attack in the realistic scenario described above (without any assumptions on model training, data distribution, or member ratio). As shown in Tab. 1, reference-model attacks such as LiRA and RMIA struggle severely in this regime: at 0.0% False Positive Rate (FPR), LiRA achieves only 0.17% True Positive Rate (TPR) on CIFAR-10, and RMIA 0.01%. Importantly, these are the best-performing attacks, even compared to white-box methods, when the knowledge assumptions are provided (see Tab. T7 in the appendix). Their effectiveness relies on training large sets of reference models under matching conditions, a requirement that breaks down when the attacker cannot replicate the target’s training process. In contrast, *ImpMIA* avoids training reference models entirely, and maintains strong TPR at low FPR across all

Attack	VGG16			ResNet50		
	AUC	@0.01 %	@0.0 %	AUC	@0.01 %	@0.0 %
<i>LiRA</i>	0.75	0.62	0.18	0.79	1.02	0.26
<i>RMIA</i>	0.78	0.69	0.06	0.78	0.09	0.02
Ours	0.78	1.59	0.56	0.82	1.80	0.78

Table 2. **Membership Inference results on different architectures (No-Auxiliary-Knowledge setting)**. Performance of LiRA, RMIA, and our method on VGG16 and ResNet50. We report AUC and TPR at fixed false-positive rates (FPR = 0.01% and 0.0%).

Method		Full Auxiliary-Knowledge	Unknown Training Config.	Different Distribution	Unknown Fraction of Members	NO Auxiliary-Knowledge
TPR @ 0.01 / 0.0%	<i>Attack-R</i>	4.62 / 1.81	1.62 / 0.37	3.27 / 1.42	2.42 / 0.0	0.31 -93.3% / 0.0 -100%
	<i>LiRA</i>	7.59 / 5.03	5.81 / 3.47	3.73 / 1.84	5.70 / 2.82	2.27 -70.1% / 0.66 -86.9%
	<i>RMIA</i>	0.24 / 0.08	0.92 / 0.32	0.28 / 0.08	0.34 / 0.06	0.15 -37.5% / 0.03 -62.5%
	ImpMIA (ours)	3.67 / 2.28	3.67 / 2.28	3.28 / 2.69	5.19 / 1.96	5.32 / 2.47

Table 3. **Evaluation of assumptions influence.** CINIC-10 membership inference across five scenarios: Auxiliary-Knowledge Setting (all assumptions), removal of each assumption individually, and removal of all three simultaneously. Each entry shows TPR (%) at 0.01% / 0.0% FPR. The last column reports relative % of performance drop with respect to the Full Auxiliary-Knowledge Setting.

datasets. On CIFAR-10, our attack achieves 1.41% TPR at 0.0% FPR, and 2.76% at 0.01% FPR, with similar or larger gains on the other datasets. Our approach achieves substantially stronger performance at strict low-FPR operating points, which are the most relevant in practical membership inference scenarios, and comparable AUC results. ROC curves are shown for CIFAR-10 in Fig. 3 and for CIFAR-100 and CINIC-10 in Fig. S2. Importantly, our attack is computationally much cheaper than reference-based methods, as it does not require training reference models and is about 4x faster than reference-model attacks (see App. B.8). Finally, Tab. 2 shows that ImpMIA outperforms prior attacks on VGG16 and ResNet50 in the low-FPR regime.

6.2. Assumptions Influence Analysis

We present a detailed analysis of the influence of removing each assumption, individually and jointly, on attack performance. As discussed earlier, reference-model-based methods rely on training reference models under conditions that closely match the target model. Their effectiveness comes from approximating the loss distributions of members versus non-members, which requires alignment between target and reference training.

In Tab. 3 we report results on the CINIC-10 dataset across five scenarios: all assumptions provided (Full Auxiliary-Knowledge setting), the removal of each assumption individually, and the removal of all three assumptions simultaneously. As shown, all methods except our proposed *ImpMIA*, which does not rely on any reference models, suffer substantial drops in performance when all assumptions are removed. In particular, *LiRA* and *Attack-R* exhibit a clear degradation as assumptions are removed. While they perform well in the Full Auxiliary-Knowledge setting, their TPR at low FPR decrease substantially under unknown configuration, distribution shift, and unknown ratio. In contrast, our method achieves strong results in these settings, as it does not depend on such assumptions. We observed improvements in *ImpMIA* at 0.01% FPR level when the fraction of members was changed, which may be explained by the evaluation metric’s dependence on the pool size (see App. B.4). It is worth noting that *RMIA*’s performance in the Full Auxiliary-Knowledge setting is lower than those reported in its original

paper. This is because our training follows the white-box setup from [Cohen & Giryes \(2024\)](#), which differs from *RMIA*’s original experimental setting. This may imply limited generalization of *RMIA* (see App. C.1 for further discussion).

6.3. Ablation and Analysis

The Appendix presents additional ablation studies and analyses. This includes: visualizations of the λ values (App. B.1); applicability to large candidate pools (App. B.2); performance under partial training-set coverage (App. B.3); the effect of pool size on evaluation (App. B.4); ablations on the scoring and aggregation components (App. B.5), the effect of weight decay (App. B.6) and pre-filtering strategies (App. B.7), and running time analysis (App. B.8).

7. Conclusion

ImpMIA advances Membership Inference by introducing a simple theory-driven white-box attack which leverages the implicit bias in neural-nets. It outperforms both black- and white-box baselines in scenarios where the attacked network’s training procedure & settings are unknown. By resorting to pure optimization of KKT conditions on the attacked model’s parameters (without the need to train any reference models), our method allows efficient scaling to very large candidate pools (see App. B.2). The white-box assumption is increasingly realistic as many modern models are publicly released with their full parameters. *ImpMIA* is best suited for scenarios where the training-set is contained in the examined-set. However, we show that this assumption can be relaxed (App. B.3), and that *ImpMIA* is competitive even at low coverage of the training-set (only 10%), and becomes superior at high coverage. Our work is the first to demonstrate the implications of implicit bias theory to membership inference attacks. More broadly, it provides a concrete case study of how insights from implicit bias theory, which have largely been developed in idealized or small-scale settings, can be instantiated in practical machine learning tasks, going beyond theory and toy examples to real datasets, larger neural networks, and standard training regimes. *ImpMIA* provides a step forward in practical privacy auditing, establishing a bridge between implicit bias theory and applied machine learning.

Acknowledgments

This research was funded by the European Union (ERC grant No. 101142115). GV is supported by the Israel Science Foundation (grant No. 2574/25), by a research grant from Mortimer Zuckerman (the Zuckerman STEM Leadership Program), and by research grants from the Center for New Scientists at the Weizmann Institute of Science, and the Shimon and Golde Picker – Weizmann Annual Grant.

References

- Buzaglo, G., Haim, N., Yehudai, G., Vardi, G., Oz, Y., Nikankin, Y., and Irani, M. Deconstructing data reconstruction: Multiclass, weight decay and general losses. *Advances in Neural Information Processing Systems*, 36: 51515–51535, 2023.
- Carlini, N., Chien, S., Nasr, M., Song, S., Terzis, A., and Tramèr, F. Membership inference attacks from first principles. In *2022 IEEE symposium on security and privacy (SP)*, pp. 1897–1914. IEEE, 2022.
- Cohen, G. and Giryes, R. Membership inference attack using self influence functions. In *Proceedings of the IEEE/CVF Winter Conference on Applications of Computer Vision*, pp. 4892–4901, 2024.
- Darlow, L. N., Crowley, E. J., Antoniou, A., and Storkey, A. J. Cinic-10 is not imagenet or cifar-10. In *NeurIPS Workshop on Machine Learning Systems (MLSys)*, 2018.
- Haim, N., Vardi, G., Yehudai, G., Shamir, O., and Irani, M. Reconstructing training data from trained neural networks. *Advances in Neural Information Processing Systems*, 35: 22911–22924, 2022.
- Jayaraman, B., Wang, L., Evans, D., Gu, L., and Hong, Y. Revisiting membership inference under realistic assumptions. *Proceedings on Privacy Enhancing Technologies*, 2021(2):348–368, 2021.
- Ji, Z. and Telgarsky, M. Directional convergence and alignment in deep learning. *Advances in Neural Information Processing Systems*, 33:17176–17186, 2020.
- Kuznetsova, A., Rom, H., Alldrin, N., Uijlings, J., Krasin, I., Pont-Tuset, J., Kamali, S., Popov, S., Mallocci, M., Kolesnikov, A., Duerig, T., and Ferrari, V. The open images dataset v4: Unified image classification, object detection, and visual relationship detection at scale. *International Journal of Computer Vision (IJCV)*, 128:1956–1981, 2020.
- Leino, K. and Fredrikson, M. Stolen memories: Leveraging model memorization for calibrated {White-Box} membership inference. In *29th USENIX security symposium (USENIX Security 20)*, pp. 1605–1622, 2020.
- Li, Z. and Zhang, Y. Membership leakage in label-only exposures. In *Proceedings of the 2021 ACM SIGSAC Conference on Computer and Communications Security*, pp. 880–895, 2021.
- Lyu, K. and Li, J. Gradient descent maximizes the margin of homogeneous neural networks. *arXiv preprint arXiv:1906.05890*, 2019.
- Nasr, M., Shokri, R., and Houmansadr, A. Comprehensive privacy analysis of deep learning: Passive and active white-box inference attacks against centralized and federated learning. In *2019 IEEE symposium on security and privacy (SP)*, pp. 739–753. IEEE, 2019.
- Neyshabur, B., Bhojanapalli, S., McAllester, D., and Srebro, N. Exploring generalization in deep learning. *Advances in neural information processing systems*, 30, 2017.
- Oz, Y., Yehudai, G., Vardi, G., Antebi, I., Irani, M., and Haim, N. Reconstructing training data from real world models trained with transfer learning. *arXiv preprint arXiv:2407.15845*, 2024.
- Peng, Y., Roh, J., Maji, S., and Houmansadr, A. Oslo: One-shot label-only membership inference attacks. In *Advances in Neural Information Processing Systems, NeurIPS 2024*, 2024. doi: 10.52202/079017-1991.
- Pradhan, G., Jälkö, J., Tobaben, M., and Honkela, A. Hyperparameters in score-based membership inference attacks. In *2025 IEEE Conference on Secure and Trustworthy Machine Learning (SaTML)*. IEEE, 2025. doi: 10.48550/arXiv.2502.06374. Accepted for publication at SaTML 2025.
- Sablayrolles, A., Douze, M., Schmid, C., Ollivier, Y., and Jégou, H. White-box vs black-box: Bayes optimal strategies for membership inference. In *International Conference on Machine Learning*, pp. 5558–5567. PMLR, 2019.
- Salem, A., Zhang, Y., Humbert, M., Berrang, P., Fritz, M., and Backes, M. MI-leaks: Model and data independent membership inference attacks and defenses on machine learning models. In *Network and Distributed Systems Security Symposium (NDSS)*, 2019.
- Shi, Y., Kotevska, O., Reshniak, V., and Sadovnik, A. Assessing membership inference attacks under distribution shifts. In *Proceedings of the 2024 IEEE International Conference on Big Data (BigData)*, pp. 4127–4131. IEEE, 2024. doi: 10.1109/BigData62323.2024.10825580.
- Shokri, R., Stronati, M., Song, C., and Shmatikov, V. Membership inference attacks against machine learning models. In *2017 IEEE symposium on security and privacy (SP)*, pp. 3–18. IEEE, 2017.

- Smorodinsky, G., Vardi, G., and Safran, I. Provable privacy attacks on trained shallow neural networks. *arXiv preprint arXiv:2410.07632*, 2024.
- Song, L. and Mittal, P. Systematic evaluation of privacy risks of machine learning models. In *30th USENIX Security Symposium (USENIX Security 21)*, pp. 2615–2632, 2021.
- Suri, A., Zhang, X., and Evans, D. Do parameters reveal more than loss for membership inference? *Transactions on Machine Learning Research (TMLR)*, 2024. URL <https://arxiv.org/abs/2406.11544>.
- Vardi, G. On the implicit bias in deep-learning algorithms. *Communications of the ACM*, 66(6):86–93, 2023.
- Wu, Y., Qiu, H., Guo, S., Li, J., and Zhang, T. You only query once: An efficient label-only membership inference attack. In *Proceedings of the International Conference on Learning Representations, ICLR 2024, 2024*. URL <https://openreview.net/forum?id=7WsivwyHrS>.
- Ye, J., Maddi, A., Murakonda, S. K., Bindschaedler, V., and Shokri, R. Enhanced membership inference attacks against machine learning models. In *Proceedings of the 2022 ACM SIGSAC conference on computer and communications security*, pp. 3093–3106, 2022.
- Yeom, S., Giacomelli, I., Fredrikson, M., and Jha, S. Privacy risk in machine learning: Analyzing the connection to overfitting. In *2018 IEEE 31st computer security foundations symposium (CSF)*, pp. 268–282. IEEE, 2018.
- Zarifzadeh, S., Liu, P., and Shokri, R. Low-cost high-power membership inference attacks. *arXiv preprint arXiv:2312.03262*, 2023.
- Zhang, C., Bengio, S., Hardt, M., Recht, B., and Vinyals, O. Understanding deep learning (still) requires rethinking generalization. *Communications of the ACM*, 64(3):107–115, 2021.

Appendix

A. ImpMIA Additional Implementation Details

In this section we provide further details on the implementation of our attack. The overall pipeline includes the following parts: (i) **pre-filtering** of candidate samples based on their classification margin, (ii) **augmentation** using horizontal flips, (iii) **block division** of weights for more efficient optimization, (iv) **gradient matrix construction** per block-structured gradient matrix A over the chosen model parameters, (v) **optimization** to solve the KKT conditions and learn the coefficients λ via blockwise optimization with dedicated regularization, (vi) **coefficient aggregation** across blocks into robust per-sample scores, and finally (vii) **post-processing** of the coefficient scores to derive the final per-sample score.

We first perform **pre-filtering**, where we filter out misclassified samples, since training members are more likely to be correctly predicted. For each candidate sample (x_i, y_i) , we compute its logit margin:

$$\Delta_i = \Phi_{y_i}(\theta; x_i) - \max_{j \neq y_i} \Phi_j(\theta; x_i),$$

and discard those with $\Delta_i < 0$. For each remaining sample we apply **augmentation**, including both the original and its horizontal flip. This reflects the fact that most models are trained with augmentations, while keeping computational cost low by not adding further augmentations. Final scores are averaged across the augmented views of each sample.

Next is **block division**. To manage dimensionality and improve optimization, parameters are partitioned into blocks of $\sim 1.5 \times 10^5$ entries and solved one block at a time. For CIFAR-10 and CINIC-10 we include all layers, while for CIFAR-100 we restrict to the final convolutional stages, where membership signals are strongest (Nasr et al., 2019). Parameters are grouped by layer order, and filters inside each convolutional layer are grouped together, since weights from the same filter/layer share statistical properties such as sparsity and magnitude. This improves conditioning of the system. In the **gradient matrix construction** step, for each retained sample we compute the gradient of its margin w.r.t. the parameters and stack them as columns of a matrix $A \in \mathbb{R}^{p \times M}$. Both the gradient block and the target parameter vector are centered and normalized.

In the **optimization** step, for each block b with parameters $\theta_{(b)}$, we solve for coefficients $\lambda_{(b)}$ by minimizing:

$$\mathcal{L} = 1 - \cos(A_{(b)}\lambda_{(b)}, \theta_{(b)}) + \alpha \mathcal{L}_{\text{neg}} + \beta \mathcal{L}_{\text{marg}}.$$

Here, \mathcal{L}_{neg} penalizes negative entries in $\lambda_{(b)}$ (reflecting complementary slackness of the KKT equations), and $\mathcal{L}_{\text{marg}}$ down-weights high-margin points, since low-margin training samples are more likely to be memorized (Haim et al., 2022). We use cosine similarity because it removes scale sensitivity and is more robust than ℓ_2 loss, preventing non-members from being incorrectly emphasized. Optimization uses AdamW with cosine learning-rate scheduling, gradient clipping, and early stopping. Coefficients are debiased by stored column norms and z -scored within each block.

After optimizing each block separately, we perform **coefficient aggregation**. Each block j yields a coefficient vector $\lambda^{(j)}$. For each sample i , we collect $\{\lambda_i^{(j)}\}_j$, sort them, and fuse into a robust score using a trimmed mean (averaging central values while discarding extremes) and a signal-to-noise ratio (SNR, mean over standard deviation across blocks). This suppresses spurious outliers and emphasizes consistent member signals.

Finally, in the **post-processing** step, we refine the raw scores using three components: (i) **class-level margin boosting**, (ii) **sample-level margin boosting**, and (iii) **distance-based scaling**. Both boosting mechanisms adjust a sample’s score according to its margin (distance from the decision boundary), but at different granularities (class vs. individual sample). (i) **Class-level boosting** is a simple per-class rescaling step, motivated by prior work (Nasr et al., 2019) showing that some classes are systematically more vulnerable to membership inference. Our boost builds on the observation that harder classes (with lower average margins) are more likely to memorize additional samples, so an attack can potentially recover more members from these classes. Accordingly, we assign slightly higher weight to harder classes and mildly downweight easier ones via a small per-class scaling coefficient of 0.03. (ii) **Sample-level margin boosting** then refines scores within each class: following previous observations (e.g., Haim et al.) that near-boundary points are more likely to be memorized, we slightly upweight low-margin, near-boundary samples and mildly downweight very high-margin ones, using a per-sample scaling factor of 0.3. (iii) **Distance-based scaling** further penalizes deviation from the estimated class margin. We approximate the

class margin \bar{m}_c as the mean margin of the top- k highest-coefficient samples in each class, and rescale scores by dividing by $|\Delta_i - \bar{m}_c|^\eta$, where Δ_i is the margin of sample i and $\eta > 0$ controls how strongly this distance affects the rescaling (we set $\eta = 0.05$ in all experiments). This ensures that only samples whose margins are consistent with typical member behavior retain high scores, helping to reduce false positives among non-members.

Layer Selection for CIFAR-100. For CIFAR-10 and CINIC-10 we construct the gradient matrix A from all convolutional layers of the network. For CIFAR-100, however, we restrict A to the final convolutional stages. This choice is motivated by both prior work and empirical observations. Nasr et al. (2019) empirically observed that, in deep CNNs trained on CIFAR-100, the strongest membership signals reside in the gradients of the later layers, while earlier layers mostly learn generic low- and mid-level features that generalize well and leak relatively little membership information. In a many-class regime such as CIFAR-100, early and mid-level layers must be heavily shared across classes, whereas the final convolutional blocks and classifier head implement sharp, class-specific decision boundaries and absorb most of the memorization.

Hyperparameter Selection. All hyperparameters of *ImpMIA* were selected using a held-out evaluation set. For CIFAR-10 and CINIC-10 we used a dedicated validation split constructed from CINIC-10, which is large enough to provide an independent validation pool. For CIFAR-100 we used a validation split taken from the generated candidate set. For each dataset, we followed the same protocol as in our main experiments: we trained 5 target models with different random seeds (affecting both the data split and the initialization) under the realistic No-Auxiliary-Knowledge setting, and ran *ImpMIA* for a small grid of hyperparameter configurations. We then selected the configuration that achieved the best average performance across these 5 runs according to our main evaluation criteria (TPR at low FPR). The same hyperparameters are used across all scenarios and across all architectures (ResNet-18, VGG16, and ResNet50).

B. Additional Ablation and Analysis

In this section, we provide further ablations and analyses of our approach: (i) visualization of the λ scores across different classes (App. B.1); (ii) scalability to large candidate pools (App. B.2); (iii) the effect of training-set coverage in the evaluated set (App. B.3); (iv) the effect of the non-member ratio and pool size on evaluation (App. B.4); (v) ablations of the scoring and aggregation variants (App. B.5); (vi) the influence of weight decay (App. B.6); (vii) the influence of pre-filtering on performance (App. B.7); and (viii) an analysis of the running time (App. B.8).

B.1. Visualization of λ Scores.

In Fig. S1, we present results for six different CIFAR-100 classes. The plots show the λ score on the y-axis and the distance from the decision boundary on the x-axis. As expected, high λ scores are strong indicators of membership. Samples very close to the decision boundary are more likely to be non-members, while almost all members with high λ values fall slightly farther from the decision boundary. This is consistent with the fact that models are trained to push training samples away from the decision boundary creating a margin, while hard test samples can lie closer to it. Interestingly, training samples that remain close to the margin are those that the network tends to memorize (Haim et al., 2022), and therefore receive higher λ scores, reflecting their strong influence on the model’s predictions and weights.

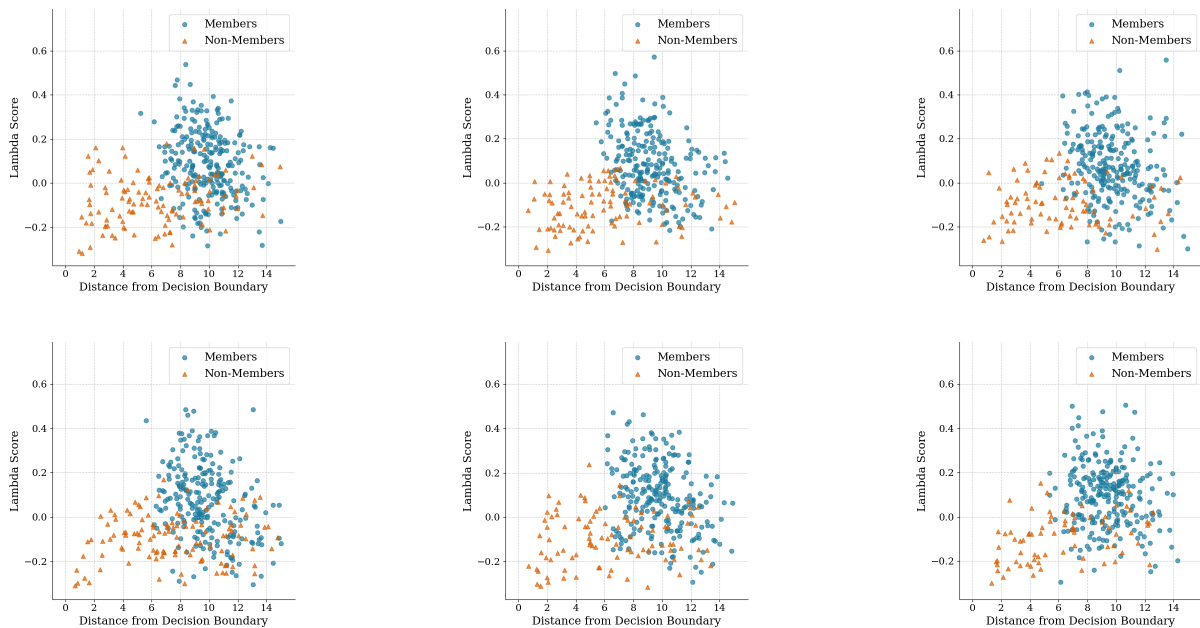


Figure S1. **Lambda scores visualization (CIFAR-100)**. Scatter plots for six different classes. Each plot shows the evaluation samples; x-axis is distance from the decision boundary, y-axis is the λ score, and points are colored by membership (member vs. non-member). High λ values strongly indicate membership.

B.2. Large Candidate Pool

We further evaluated ImpMIA under larger candidate pools. In addition to the 50,000 ($\approx 2\times$) and 80,000 ($\approx 3\times$) candidate sets reported in the main text, we consider a pool of 250,000 candidates ($\approx 10\times$ the training size) on CIFAR-10. Following our realistic no auxiliary knowledge protocol, the target model is trained on 25,000 CIFAR-10 samples, while the reference set consists of the remaining 25,000 CIFAR-10 samples together with 200,000 images from CINIC-10. As shown in Table T1, ImpMIA achieves TPRs of 3.00% at 0.01% FPR and 0.54% at 0.0% FPR, substantially outperforming other MIAs at low FPRs in the larger candidate pool scenario.

Attack	AUC	@0.01 %	@0.0 %
<i>Attack-R</i>	0.75	0.01	0.0
<i>Attack-P</i>	0.76	0.12	0.0
<i>LiRA</i>	0.80	0.54	0.11
<i>Ours</i>	0.79	3.00	0.54

Table T1. **Membership inference with a 250K candidate pool (CIFAR-10).** We compare ImpMIA to other MIA baselines under the realistic No-Auxiliary-Knowledge setting. We report AUC and TPR at fixed false-positive rates (FPR = 0.01% and 0.0%).

B.3. Effect of Training Sample Coverage in the Evaluation Set

Our method relies on the implicit bias of the network, linking training samples to the learned weights. Consequently, if a large portion of the training set is missing from the evaluation set, performance naturally decreases. Importantly, in practice it is reasonable to expect evaluation set that cover most of the training set, especially since our method’s efficiency allows scaling to very large candidate pools without the need to train reference models. As shown in Tab. T2, for the No-Auxiliary-Knowledge setting performance is strongest when most of the training set is included, but our attack also works well under partial training coverage. In all cases, evaluation is on a random 8,000 (10%) samples from the candidate pool to avoid influence from candidate pool size on the reported metrics.

In Tab. T3 we show a direct comparison with the previous best methods under only 10% coverage in our realistic scenario. Even with this low coverage, our results are comparable to the best competitors, and with higher coverage our method clearly surpasses them (Tab. 1). Higher coverage is a likely scenario in many practical settings, such as auditing whether a specific dataset was used to train a model, or when a dataset is known to contain the training set but the exact subset used is unknown..

Coverage	CIFAR-10		
	AUC	@0.1 %	@0.0 %
100%	0.81	6.80	2.26
75%	0.81	5.49	1.42
50%	0.81	5.34	1.61
25%	0.79	3.49	0.96
10%	0.75	3.01	0.94

Table T2. **Effect of training sample coverage (no auxiliary knowledge).** Ablation study on CIFAR-10 showing the impact of training sample coverage within the candidate superset. Performance is strongest when most of the training set is included, but our method remains effective under partial coverage.

Attack	AUC	@0.1 %	@0.0 %
<i>Attack-P</i>	0.76	0.38	0.06
<i>Attack-R</i>	0.74	1.73	0.32
<i>LiRA</i>	0.80	2.98	1.20
<i>RMIA</i>	0.80	2.43	0.14
<i>Ours</i>	0.75	3.01	0.94

Table T3. **Comparison under limited coverage of 10% (no auxiliary knowledge).** We compare our method on CIFAR-10 with previous attacks when the candidate superset covers only 10% of the training data in our realistic No-Auxiliary-Knowledge setting. Even under this low coverage, our results are comparable to the best competitors.

B.4. Influence of Non-Member Ratio on Evaluation

Our assumption-removal analysis also showed the influence of candidate pool size on model performance. In this setting, we lowered the member ratio by adding more non-members to the superset (increasing from 25K to 55K non-members). While our method does not rely on any specific member-to-non-member ratio, adding more non-members can affect results in two ways: (i) it increases the number of samples, which may make it harder to classify members, and (ii) it directly affects the evaluation metric, since FPR is defined relative to the total number of non-member samples. The overall performance reflects the interaction of these two factors. On the one hand, a larger pool introduces more distractors, potentially reducing accuracy. On the other hand, at fixed FPR thresholds (e.g., 0.01%), a larger pool allows more absolute mistakes. For instance, with 25K non-members, 0.01% FPR corresponds to only two false positives, whereas with 55K non-members, it allows up to five. Since coefficients are not uniformly distributed, permitting more mistakes can yield a nonlinear gain in TPR. In practice, we observed that at 0.01% FPR, our method performed better with 55K non-members than with 25K. This suggests that the positive effect of the evaluation metric outweighs the negative impact of additional distractors. Importantly, at 0.0% FPR, where the metric is unaffected by pool size, the results remained stable, as expected.

B.5. Scoring Variants Ablation

We present an ablation study of the different score-refinement components in our pipeline for CIFAR-10 in our No-Auxiliary-Knowledge setting (see Tab. T4). After block-wise optimization, each sample has multiple coefficient estimates, one per block, which are fused into a robust score using both a trimmed mean (to discard extreme outliers) and a signal-to-noise ratio (SNR, mean over standard deviation across blocks). This aggregation step already improves robustness by emphasizing consistent membership signals. On top of this, we evaluate margin-based boosting and distance scaling. Class-level boosting gives higher weight to harder classes (with lower average margins), while per-sample boosting highlights points near the decision boundary, which are more likely to be memorized. Finally, distance scaling penalizes samples whose margins deviate from the estimated class margin, reducing false positives. As shown, each component contributes to performance gains, and the full *ImpMIA* pipeline achieves the strongest low-FPR detection. Moreover, with either aggregation option, and even without any post-processing, our attack already outperforms previous attacks and shows strong results. The post-processing steps have only a comparatively small influence at low FPR (e.g., TPR@0.0% ranges only from 1.23 to 1.41), while aggregation has a larger effect. This is expected, since aggregation determines how we exploit the main signal produced by the KKT-based optimization. Overall, the primary source of our gains comes from the implicit-bias-based optimization itself rather than from the specific post-processing.

Variant	AUC	@0.01 %	@0.0 %
<i>Trimmed mean only</i>	0.74	2.58	1.18
<i>Robust SNR only</i>	0.85	2.51	0.89
<i>Fusion (trimmed mean + SNR)</i>	0.82	2.60	1.23
+ <i>Boost1 (class-level margins)</i>	0.82	2.59	1.23
+ <i>Boost2 (sample-level margins)</i>	0.81	2.69	1.39
+ <i>Trim division</i>	0.82	2.84	1.31
<i>ImpMIA</i>	0.81	2.76	1.41

Table T4. Ablation of ImpMIA components for CIFAR-10 (no auxiliary knowledge). Performance of different scoring variants and incremental boosts. We report AUC and TPR at fixed false-positive rates (FPR = 0.01% and 0.0%).

B.6. Weight Decay Influence

To study the effect of explicit weight decay, we evaluated *ImpMIA* on CIFAR-10 No-Auxiliary-Knowledge setting, both with the standard decay level (10^{-4}) and without decay. While the KKT stationarity formulation applies in the homogeneous case, prior theory suggests that in non-homogeneous networks explicit weight decay is needed as a replacement. However, our results show that even in this setting the attack remains effective without weight decay: the no-weight decay variant achieves the same AUC (0.81) and slightly stronger performance in the low-FPR regime (2.93 vs. 2.76 at 0.01% FPR; 1.62 vs. 1.41 at 0.0% FPR). This is consistent with the intuition that stronger regularization can suppress memorization and weaken membership signals. Overall, this demonstrates the robustness of our method and that weight decay is not strictly necessary for strong empirical performance.

Variant	CIFAR-10		
	AUC	@0.01 %	@0.0 %
Without weight decay	0.81	2.93	1.62
10^{-4}	0.81	2.76	1.41

Table T5. **Effect of Weight Decay (no auxiliary knowledge)**. Ablation on CIFAR-10 comparing the standard weight decay level (10^{-4}) to training without weight decay. Although implicit bias theory assumes weight decay in the non-homogeneous case for the KKT characterization, our results show the attack remains effective regardless.

B.7. Influence of Pre-Filtering

The pre-filtering step aims to both stabilize the optimization by eliminating samples that are unlikely to be members (and therefore may add noise) and speed up optimization by having fewer samples. On the other hand, it may discard data points that are hard to learn even though they were in the training data, and therefore miss member samples. Since any attack is likely to miss some members, this is a trade-off that can be chosen in practice.

We analyze the impact of the pre-filtering step on our method’s performance in the CIFAR-10 No-Auxiliary-Knowledge setting. On CIFAR-10, pre-filtering removes between 4–25% of the examples, depending on the seed and scenario. As shown in Tab. T6, using pre-filtering leads to a slight increase in AUC (from 0.78 to 0.81), as well as improvements in TPR at 0.01% FPR (from 2.28 to 2.76) and at 0.0% FPR (from 1.15 to 1.41). Overall, the pre-filtering step does not appear to have a significant influence on performance, but it does speed up optimization by reducing the number of points being optimized

Variant	AUC	@ 0.01% FPR	@ 0.0% FPR
No pre-filtering	0.78	2.28	1.15
With pre-filtering	0.81	2.76	1.41

Table T6. **Effect of pre-filtering on ImpMIA (CIFAR-10, no auxiliary knowledge)**. Comparison of AUC and TPR at very low FPR with and without the pre-filtering step. We report AUC and TPR at fixed false-positive rates (FPR = 0.01% and 0.0%).

B.8. Running Time

The runtime of *ImpMIA* ranges between 12–16 hours on a single H200 GPU, depending on the size of the candidate pool (50K–80K samples), and can be reduced to approximately 2 hours using 8 GPUs. The black-box reference-model attacks in their strongest setting, used in this paper as well, require training 256 reference models. In the Full Auxiliary-Knowledge setting (400 epochs with a candidate pool of size 50K), this results in a total runtime of approximately 48 hours on a single GPU, which is roughly $4\times$ slower than *ImpMIA*. Notably, the runtime of black-box reference-model attacks is highly influenced by the number of epochs assumed by the attacker to mimic the target model’s training (which can be both lower or much higher than 400). In contrast, the runtime of *ImpMIA* remains largely unchanged, as it requires no reference model training.

C. Competitive Baselines: Technical Details

C.1. Black-Box Baselines

For black-box comparisons, we used the official **RMIA** implementation, which also includes code for **LiRA**, **Attack-P**, and **Attack-R**. We ran the *full-power* RMIA variant described by [Zarifzadeh et al. \(2023\)](#), which trains 256 reference models per dataset, and used the same framework to evaluate the other black-box baselines. To ensure consistency, we adapted the code to match the training configuration of [Cohen & Giryas \(2024\)](#) (SIF): ResNet-18 backbone, inputs normalized to $[0, 1]$, and standard augmentations (random crop and horizontal flip).

RMIA requires dataset-specific configurations, which we followed exactly as provided in their code and paper for CIFAR-10, CIFAR-100, and CINIC-10. All experiments were therefore run with the recommended hyperparameters for each dataset. We emphasize that RMIA, despite reporting state-of-the-art results in its original paper, is highly sensitive to training configurations, especially at very low false-positive rates. Even minor mismatches in normalization, architecture, optimizer, or learning-rate schedule caused severe degradation in our experiments.

C.2. White-Box Baselines

Gradient-based Baselines. ([Nasr et al., 2019](#)) showed that the most informative white-box membership signal is the magnitude of per-sample gradients, since stochastic gradient descent drives member gradients toward zero. Building on this, we evaluate two baselines: (i) a *loss-gradient* score based on the gradients of the loss $\|\nabla_{\theta} L(f(x), y)\|$, and (ii) a *margin-gradient* score based on the gradients of the margin $\|\nabla_{\theta}[f_y(x) - \max_{j \neq y} f_j(x)]\|$. For each sample (and its horizontal flip), we compute per-layer gradient norms, convert them into rank-based scores (higher rank = smaller norm), and average across layers and augmentations. The loss-gradient baseline directly instantiates ([Nasr et al., 2019](#)) observation, while the margin-gradient baseline adapts it to sensitivity around the margin, making it conceptually closer to *ImpMIA*.

SIF Attack. The self-influence function (SIF) attack of [Cohen & Giryas \(2024\)](#) achieved state-of-the-art white-box membership inference in their paper, particularly under strong augmentations where gradient-norm methods fail. SIF measures a sample’s effect on its own loss by approximating the influence function via recursive Hessian–vector products. Membership is inferred by whether a correctly classified sample’s score lies close to zero, since training points tend to cluster tightly around this value while non-members yield more extreme values.

The original SIF formulation assumes access to labeled calibration samples to set the decision thresholds, and results were reported only on small subsets of data (500 calibration, 2,500 evaluation), producing binary member/non-member predictions. In our setting, however, no labeled calibration samples are available, and we require continuous membership scores to compute TPR at low FPR across the full evaluation pool. We therefore adapt the method with a simple *distance-to-zero* criterion: the closer a score is to zero, the stronger the evidence of membership. To stabilize the Hessian inversion, we use four recursion steps and average over four stochastic estimates. This reduced setting makes the attack faster while remaining stable across the full evaluation pool.

C.3. Additional Results

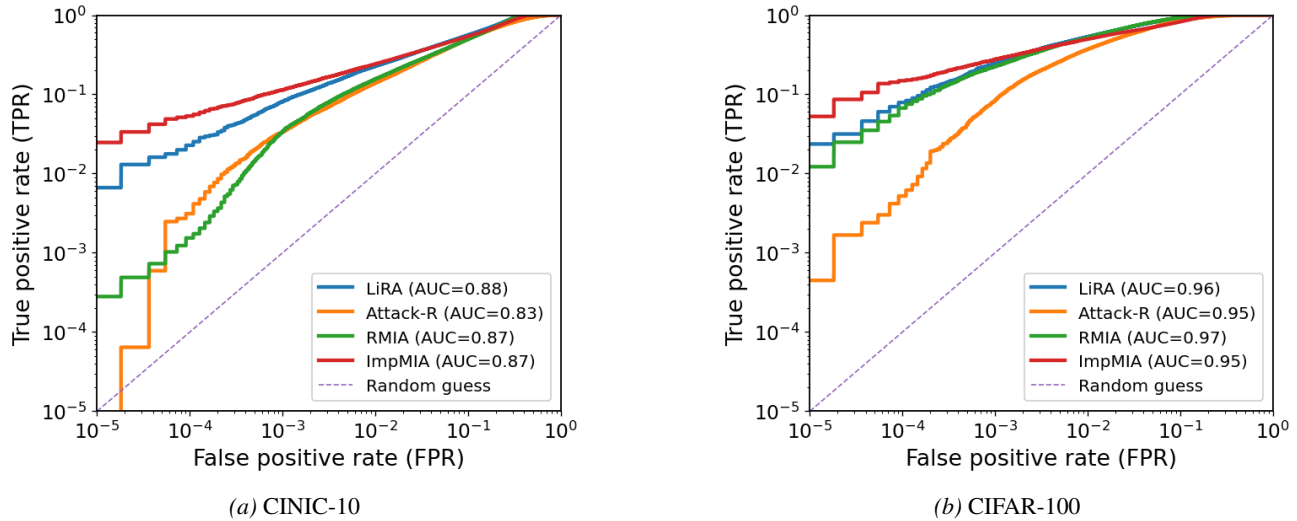


Figure S2. **TPR-FPR plots for the No-Auxiliary-Knowledge setting.** These curves illustrate attack performance when the attacker faces realistic uncertainty: (i) training hyperparameters are unknown, (ii) the candidate pool mixes in- and out-of-distribution samples (distribution shift), and (iii) the fraction of members is unknown. The plots complement the main text by showing the full ROC behavior, especially in the low-FPR regime.

Attack	CIFAR-10			CIFAR-100			CINIC-10		
	AUC	@0.01 %	@0.0 %	AUC	@0.01 %	@0.0 %	AUC	@0.01 %	@0.0 %
<i>Attack-P</i>	0.59	0.01	0.0	0.81	0.0	0.0	0.70	0.0	0.0
<i>Attack-R</i>	0.67	2.56	1.58	0.88	19.04	16.07	0.78	4.62	1.81
<i>LiRA (online)</i>	0.75	5.28	3.56	0.95	24.26	15.25	0.86	7.59	5.03
<i>LiRA (offline)</i>	0.58	1.94	0.74	0.81	5.88	2.44	0.69	2.59	1.17
<i>RMIA (online)</i>	0.74	1.48	0.69	0.94	14.69	8.46	0.84	0.24	0.08
<i>RMIA (offline)</i>	0.73	3.47	1.83	0.93	25.98	20.44	0.83	0.24	0.10
<i>GradNorm - loss</i>	0.61	0.01	0.0	0.83	0.01	0.0	0.74	0.0	0.0
<i>GradNorm - margin</i>	0.59	0.0	0.0	0.72	0.04	0.01	0.69	0.01	0.0
<i>AdaSIF</i>	0.62	0.01	0.0	0.87	0.03	0.01	0.75	0.0	0.0
Ours	0.71	1.48	0.90	0.90	9.66	6.73	0.82	3.67	2.28

Table T7. **Membership Inference results (full auxiliary knowledge).** Performance across all datasets under the assumption-rich setting where training hyperparameters, data distribution, and member ratio are known. Metrics reported are TPR (%) at 0.0% and 0.01% FPR, with AUC included for completeness.

Attack	CINIC-10		
	AUC	@0.01 %	@0.0 %
<i>Attack-P</i>	0.71	0.01	0.0
<i>Attack-R</i>	0.76	2.42	0.0
<i>LiRA (online)</i>	0.85	5.70	2.82
<i>LiRA (offline)</i>	0.58	0.41	0.12
<i>RMIA (online)</i>	0.83	0.34	0.06
<i>RMIA (offline)</i>	0.83	0.41	0.07
<i>Ours</i>	0.81	5.19	1.96

Table T8. **Membership Inference results (unknown fraction of members)**. CINIC-10 results when the attacker does not know the proportion of training members in the candidate pool. Metrics reported are TPR (%) at 0.0% and 0.01% FPR, plus AUC.

Attack	CIFAR-10			CIFAR-100			CINIC-10		
	AUC	@0.01 %	@0.0 %	AUC	@0.01 %	@0.0 %	AUC	@0.01 %	@0.0 %
<i>Attack-P</i>	0.75	0.03	0.0	0.90	0.02	0.0	0.82	0.01	0.0
<i>Attack-R</i>	0.71	1.02	0.63	0.93	10.10	4.95	0.82	3.27	1.42
<i>LiRA (online)</i>	0.81	1.94	1.14	0.97	12.66	4.63	0.90	3.73	1.84
<i>LiRA (offline)</i>	0.53	0.04	0.01	0.76	0.0	0.0	0.70	0.31	0.17
<i>RMIA (online)</i>	0.80	0.34	0.05	0.97	10.83	5.54	0.88	0.28	0.08
<i>RMIA (offline)</i>	0.79	0.56	0.14	0.97	15.36	8.50	0.86	0.51	0.15
<i>Ours</i>	0.81	2.14	1.18	0.95	11.60	5.05	0.85	3.28	2.69

Table T9. **Membership Inference results (different data distribution)**. Performance across all datasets when the candidate pool mixes in-distribution and out-of-distribution data. Metrics reported are TPR (%) at 0.0% and 0.01% FPR, with AUC included for completeness.

Attack	CIFAR-10			CIFAR-100			CINIC-10		
	AUC	@0.01 %	@0.0 %	AUC	@0.01 %	@0.0 %	AUC	@0.01 %	@0.0 %
<i>Attack-P</i>	0.59	0.01	0.0	0.81	0.01	0.0	0.71	0.0	0.0
<i>Attack-R</i>	0.67	1.53	0.49	0.90	2.97	1.55	0.79	1.62	0.37
<i>LiRA (online)</i>	0.73	2.56	1.32	0.92	13.86	9.93	0.85	5.81	3.47
<i>LiRA (offline)</i>	0.62	0.98	0.38	0.88	5.43	2.26	0.72	1.69	1.03
<i>RMIA (online)</i>	0.72	1.65	0.46	0.93	6.49	0.84	0.84	0.92	0.32
<i>RMIA (offline)</i>	0.71	1.89	0.76	0.92	15.14	9.99	0.83	0.79	0.08
<i>Ours</i>	0.71	1.48	0.90	0.90	9.66	6.73	0.82	3.67	2.28

Table T10. **Membership Inference results (unknown training configuration)**. Performance across all datasets when the attacker does not know the target model’s training hyperparameters. Metrics reported are TPR (%) at 0.0% and 0.01% FPR, with AUC included for completeness.

Attack	CIFAR-10			CIFAR-100			CINIC-10		
	AUC	@0.01 %	@0.0 %	AUC	@0.01 %	@0.0 %	AUC	@0.01 %	@0.0 %
<i>LiRA (online)</i>	0.80	0.55	0.17	0.96	7.90	2.36	0.88	2.27	0.66
<i>LiRA (offline)</i>	0.49	0.0	0.0	0.76	0.0	0.0	0.64	0.04	0.02
<i>RMIA (online)</i>	0.80	0.19	0.01	0.97	6.73	1.22	0.87	0.15	0.03
<i>RMIA (offline)</i>	0.79	0.26	0.0	0.97	7.35	1.67	0.86	0.11	0.02

Table T11. **LiRA and RMIA: offline vs. online (no auxiliary knowledge)**. Results for LiRA and RMIA across all datasets in the realistic no-auxiliary-knowledge setting. The offline variant trains reference models independently of the candidate superset, while the online variant trains reference models directly on subsets of the superset, closer to the evaluation setup. Metrics reported are TPR (%) at 0.0% and 0.01% FPR, with AUC included for completeness.

Attack	CIFAR-10		CIFAR-100		CINIC-10	
	@0.01 %	@0.0 %	@0.01 %	@0.0 %	@0.01 %	@0.0 %
<i>Attack-P</i>	0.02 ± 0.0	0.0 ± 0.0	0.01 ± 0.0	0.0 ± 0.0	0.01 ± 0.0	0.0 ± 0.0
<i>Attack-R</i>	0.23 ± 0.10	0.04 ± 0.04	0.52 ± 0.14	0.04 ± 0.01	0.31 ± 0.19	0.0 ± 0.0
<i>LiRA</i>	0.55 ± 0.09	0.17 ± 0.01	7.90 ± 0.79	2.36 ± 0.30	2.27 ± 0.25	0.66 ± 0.13
<i>RMIA</i>	0.19 ± 0.04	0.01 ± 0.0	6.73 ± 0.84	1.22 ± 0.45	0.15 ± 0.02	0.03 ± 0.0
<i>GradNorm-loss</i>	0.11 ± 0.01	0.01 ± 0.0	0.10 ± 0.02	0.04 ± 0.01	0.09 ± 0.02	0.01 ± 0.0
<i>GradNorm-margin</i>	0.02 ± 0.01	0.0 ± 0.0	0.02 ± 0.01	0.01 ± 0.0	0.03 ± 0.0	0.01 ± 0.01
<i>AdaSIF</i>	0.05 ± 0.01	0.0 ± 0.0	0.01 ± 0.0	0.0 ± 0.0	0.01 ± 0.0	0.0 ± 0.0
<i>ImpMIA (ours)</i>	2.76 ± 0.34	1.41 ± 0.29	14.86 ± 0.40	5.26 ± 1.01	5.32 ± 0.42	2.47 ± 0.46

Table T12. **Membership Inference Results (no auxiliary knowledge)**. Performance across all datasets under the realistic no-assumptions setting. Metrics reported are TPR (%) at 0.0% and 0.01% FPR, with standard error included. This table shows the same results as in Tab. 1, but with standard error values reported.

Method	Full	Unknown	Different	Unknown Fraction	NO
	Auxiliary-Knowledge	Training Config.	Distribution	of Members	Auxiliary-Knowledge
<i>Attack-R</i>	4.62 ± 0.76	1.62 ± 0.67	3.27 ± 0.53	2.42 ± 0.19	0.31 ± 0.20
<i>LiRA</i>	7.59 ± 0.47	5.81 ± 0.53	3.73 ± 0.70	5.70 ± 0.58	2.27 ± 0.25
<i>RMIA</i>	0.24 ± 0.05	0.92 ± 0.32	0.28 ± 0.15	0.34 ± 0.06	0.15 ± 0.02
<i>ImpMIA (ours)</i>	3.67 ± 0.95	3.67 ± 0.95	3.28 ± 0.41	5.19 ± 0.31	5.32 ± 0.42

Table T13. **Assumptions influence (CINIC-10, @0.01% FPR)**. Each entry is TPR (%) ± se. This table shows the same results as in Tab. 3, but with standard error values reported.

Method	Full	Unknown	Different	Unknown Fraction	NO
	Auxiliary-Knowledge	Training Config.	Distribution	of Members	Auxiliary-Knowledge
<i>Attack-R</i>	1.81 ± 0.55	0.37 ± 0.26	1.42 ± 0.80	0.0 ± 0.0	0.0 ± 0.0
<i>LiRA</i>	5.03 ± 0.89	3.47 ± 1.01	1.84 ± 0.53	2.82 ± 0.61	0.66 ± 0.14
<i>RMIA</i>	0.08 ± 0.03	0.32 ± 0.09	0.08 ± 0.03	0.06 ± 0.03	0.03 ± 0.01
<i>ImpMIA (ours)</i>	2.28 ± 0.60	2.28 ± 0.60	2.69 ± 0.53	1.96 ± 0.38	2.47 ± 0.46

Table T14. **Assumptions influence (CINIC-10, @0.0% FPR)**. Each entry is TPR (%) ± se. This table shows the same results as in Tab. 3, but with standard error values reported.

D. Binary case of the KKT equations and Implicit Bias with Weight Decay

For completeness, we also present the implicit bias of neural networks for the binary classification case, as appeared in Lyu & Li (2019); Ji & Telgarsky (2020); Haim et al. (2022); Smorodinsky et al. (2024), and its extension to training with weight decay that was previously considered in (Buzaglo et al., 2023).

Implicit bias of gradient flow in homogeneous networks: Let $\Phi(\theta; \cdot) : \mathbb{R}^d \rightarrow \mathbb{R}$ be a homogeneous ReLU network. Consider minimizing the logistic loss over a binary classification dataset $\{(x_i, y_i)\}_{i=1}^n \subseteq \mathbb{R}^d \times \{\pm 1\}$ using gradient flow. Suppose that at some time t_0 the network classifies all samples correctly. Then gradient flow converges in direction to a KKT point of the maximum-margin problem:

$$\min_{\theta} \frac{1}{2} \|\theta\|^2 \quad \text{s.t.} \quad \forall i \in [n] \quad y_i \Phi(\theta; x_i) \geq 1.$$

The associated KKT conditions are:

$$\theta - \sum_{i=1}^n \lambda_i \nabla_{\theta} [y_i \Phi(\theta; x_i)] = 0 \quad (\text{stationarity}) \quad (6)$$

$$y_i \Phi(\theta; x_i) \geq 1 \quad (\text{primal feasibility}) \quad (7)$$

$$\lambda_i \geq 0 \quad (\text{dual feasibility}) \quad (8)$$

$$\lambda_i = 0 \quad \text{if } y_i \Phi(\theta; x_i) \neq 1 \quad (\text{complementary slackness}). \quad (9)$$

Bias with weight decay: Previous works (Haim et al., 2022; Buzaglo et al., 2023) have further analyzed the effect of explicit weight decay in this context. For simplicity, and following Buzaglo et al. (2023), we present the analysis in the binary classification case, though the argument can be extended to the multiclass setting.

Let $\ell(\Phi(x_i; \theta), y_i)$ be a loss function that takes as input the scalar prediction of the model $\Phi(\cdot; \theta)$ on sample x_i , and its corresponding label y_i . The total regularized loss is

$$L(\theta) = \sum_{i=1}^n \ell(\Phi(x_i; \theta), y_i) + \lambda_{\text{WD}} \frac{1}{2} \|\theta\|^2.$$

Assuming convergence ($\nabla_{\theta} L = 0$), the parameters satisfy

$$\theta = \sum_{i=1}^n \ell'_i \nabla_{\theta} \Phi(x_i; \theta), \quad \ell'_i = -\frac{1}{\lambda_{\text{WD}}} \frac{\partial \ell(\Phi(x_i; \theta), y_i)}{\partial \Phi(x_i; \theta)}. \quad (10)$$

This relation shows that the trained weights again lie in the span of per-sample gradients, with coefficients $\{\ell'_i\}$ determined by the derivative of the loss. Importantly, (10) is structurally equivalent to the stationarity condition in the KKT system of the max-margin problem: in both formulations, the parameters are expressed as a linear combination of margin-gradient directions. Furthermore, if ℓ is the logistic loss function, then the coefficients $\{\ell'_i\}$ of this linear combination are non-negative.

E. Limitations of Average-Case Metrics

A common evaluation practice in the membership inference literature is to report average-case metrics such as balanced accuracy or ROC-AUC. While convenient, these metrics are misaligned with the privacy risks that matter in practice.

First, average-case metrics obscure worst-case behavior. Balanced accuracy treats false positives and false negatives symmetrically, yet in privacy attacks the costs are asymmetric: false positives (incorrectly labeling non-members as members) undermine reliability, whereas false negatives are typically less harmful. Second, aggregate metrics such as AUC average performance across the entire ROC curve, including regions of high false-positive rates that are irrelevant in practice. As emphasized by [Carlini et al. \(2022\)](#), an attack may achieve high AUC while completely failing to recover any members at $\leq 0.1\%$ FPR. Conversely, an attack that reliably recovers only a small subset of members may achieve modest AUC but still constitute a severe privacy breach. For this reason, recent work on membership inference ([Carlini et al., 2022](#); [Zarifzadeh et al., 2023](#)) has adopted TPR at low FPR as the primary evaluation metric.

This mismatch is evident in our results. [Table 1](#) reports performance of several attacks in the No-Auxiliary-Knowledge setting. On CIFAR-10, both our attack and the GradNorm baseline achieve $AUC \approx 0.81$. However, this similarity is misleading: GradNorm leverages model confidence, and its apparent effectiveness comes from the fact that non-members in this scenario have low confidence. By contrast, as shown by [Haim et al. \(2022\)](#), the truly memorized samples are those near the decision boundary. Our attack explicitly targets such near-margin points, yielding much higher TPR at very low FPR (e.g., 2.76% vs. 0.11% at 0.01% FPR). This gap illustrates why average-case metrics like AUC are problematic: they make GradNorm appear competitive, while in reality it fails where privacy evaluation matters most, the low-FPR regime